Nonaqueous Electrolyte Development for Electrochemical Capacitors

T. R. Jow
K. Xu
S. P. Ding

September 1999

For
U.S. Department of Energy
Assistant Secretary for
Energy Research
Washington, DC

By
U.S. Army Research Laboratory
Adelphi, MD

NONAQUEOUS ELECTROLYTE DEVELOPMENT FOR ELECTROCHEMICAL CAPACITORS

T. R. Jow
K. Xu
S. P. Ding

September 1999

Contents

Figures

Tables

Acknowledgments

Executive Summary

The U.S. Army Research Laboratory (ARL) has been actively involved in development of nonaqueous electrolytes for rechargeable lithium (Li) batteries since the early 1970s. ARL has also been engaged in the development of capacitors for pulsed-power applications since 1989. We concentrated on film capacitors originally, as we were faced with requirements for extreme high-power densities (electromagnetic launchers). We shifted to electrolytic capacitors and finally to electrochemical pseudo-capacitors based on amorphous ruthenium oxides **(1–5)** as our requirements shifted to the need for higher energy densities and more modest power densities for transportation and burst communications. With our knowledge of and experience in electrolytes and capacitors, we recently started to investigate a lower cost carbon-based double-layer capacitor using nonaqueous electrolytes. As there are similarities in the electrolytes for batteries and electrochemical capacitors, we believe that we can make a significant contribution in this area.

Electrochemical capacitors are attractive to use because of their long cycle life and inherent high-power (or fast charge/discharge) capabilities. To realize the inherent high-power nature of the capacitor, the resistance of the capacitor needs to be low. The resistance of the capacitors comes from two parts: the electronic part and the ionic part. The main focus of this project, however, is on the ionic part of capacitor resistance. The ionic resistance is largely determined by the electrolyte, especially the electrolyte's conductivity. In double-layer capacitors, the electrolyte also functions as an active material that provides the necessary ionic charges for charging the electrolyte and electrode interface. Therefore, in addition to high conductivity, a high ion concentration becomes one of the key parameters that needs to be improved for high-performance nonaqueous electrolytes.

The objectives of this project were to demonstrate and develop new nonaqueous electrolytes that enable the development of high power in excess of 2 kW/kg and high energy in excess of 8 Wh/kg capacitors. To achieve these objectives, the ideal electrolytes should possess the following characteristics:

High conductivity: σ > 20 to 40 mS/cm at room temperature
High salt concentration: C > 1.5 M
Large electrochemical stability window: ΔV > 3 V
Wide operating temperature range: –40 to 70 °C
Thermally stable: –40 to 70 °C
Environmentally benign.

To achieve the objectives of this project, two approaches were used. The first approach was to search for the proper solvent mixtures within the commercially available quaternary ammonium salts such as tetraethyl ammonium tetrafluoroborate (Et_4NBF_4) or tetraethyl ammonium hexafluorophosphate (Et_4NPF_6). The second approach was to use the commonly available solvent systems but develop new salts. We believe that we will be able to achieve our goal by using salts with proper cation and anion combinations.

In searching for the proper solvent mixtures using the commercially available salts Et_4NBF_4 and Et_4NPF_6, we found that the solubility of these salts in the solvent mixtures that we investigated does not reach our objective of having a greater than 1.5-M concentration except in acetonitrile (AN) and ethylene carbonate (EC). The solubility of Et_4NBF_4 in AN is 1.68 M at room temperature and its conductivity at room temperature is 57 mS/cm at a 1.65-M

concentration. We observed substantial improvement in power performance for Panasonic's GoldCap® capacitors over that for capacitors using the original electrolyte of 0.65 M Et_4NBF_4 in propylene carbonate (PC). However, AN's lower oxidative stability and high vapor pressure make it unsuitable for long life and high-temperature applications. Although the solubility of Et_4NBF_4 in EC is 1.625 M at room temperature, its solubility decreases substantially at low temperatures.

Our effort was then directed to the second approach, developing salts that can be dissolved more than 1.5 M in the commonly used solvent systems. We also wanted the electrolytes containing these salts to be stable with respect to electrodes at the same time. Our literature survey suggested that quaternary ammonium salts are the most stable salts compared with other classes of salts. We decided to systematically synthesize a series of quaternary ammonium salts with different asymmetric cation and anion combinations. Thus far, we have synthesized 13 different salts. We observed a substantial increase in solubility when the cation was changed from a symmetric structure such as tetraethyl ammonium to an asymetric structure such as triethylmethyl ammonium. For example, the solubility of Et_4NPF_6 in EC-DMC is 1.46 M, while the solubility of Et_3MeNPF_6 in EC-DMC is 3.13 M. The conductivity of the electrolyte containing asymmetric quaternary ammonium salts is similar to that of the electrolyte containing symmetric ones at the same salt concentration. Since the asymmetric salts can be dissolved to a greater degree, the conductivity of these electrolytes can reach a higher value than that of the symmetric ones, reaching over 20 mS/cm at room temperature.

The electrochemical stability window of the electrolyte containing new salts was slightly improved due to an improvement in the reductive stability of the cation. This improvement comes from the steric protection of the alkyl substituents. To obtain a realistic value of the stability window for a practical carbon material, the traditional method is to use an arbitrary current value as a limit to determine the voltage limit, but this does not work for the high surface area of carbon materials. A new method that uses charge, or an integration of current, instead of using current directly to detect the instability limit gave us values that more realistically reflect the true stability window. Using the new method and new salts, we learned that the stability window of the electrolyte also varies with the solvent. Our study was not exhaustive; however, it is important in that we found that the sulfone-based solvent achieved a stability window as high as 3.5 V.

A demonstration of the new electrolyte, especially Et_3MeNPF_6 in EC-DMC, using a prototype cell from Maxwell Technologies was started at the end of the project. However, the required amount of purified electrolyte and the time needed to complete the tests were beyond the scope of the present project.

In summary, we have made substantial advances in quaternary ammonium salts and identified solvent systems that can withstand high voltage operations. However, improvement in the salt alone is not sufficient. Improvements in the low-temperature stability of a capacitor rely not only on the salts but also on the solvents. Likewise, the high-temperature stability of the capacitor will depend not only on the salts but also on the solvents and carbon electrode materials. Much remains to be accomplished, especially in exploring solvents and carbon materials. The next phase of our work will require the participation of (i) a capacitor manufacturer for carbon electrode fabrication and capacitor assembly and (ii) a chemical company for electrolyte preparation and purification.

1. Introduction

1.1 The Importance of Electrolyte

The electrolyte in electrochemical capacitors is generally recognized as one of the key components that determine the ionic of the capacitor and, thus, the power capability and the deliverable energy content of the capacitor. The other component is the electronic resistance, which includes the electrodes and the cell assembly. This is beyond the scope of this report and will not be discussed here. Therefore, the conductivity of the electrolyte is our primary concern.

At ARL, our initial effort started with a search for electrolytes with conductivity higher than that of the electrolyte used in the commercially available state-of-the-art double-layer capacitors, such as Panasonic's GoldCap® capacitor. This capacitor uses 0.65 M of tetraethylammonia tetrafluoroborate in propylene carbonate (Et$_4$NBF$_4$/PC) **(6)** as an electrolyte. The conductivity of this electrolyte is only 8.8 mS/cm at room temperature. We replaced the electrolyte in the GoldCap® capacitor with the electrolyte of Et$_4$NBF$_4$ in acentonitrile (AN). This electrolyte has a conductivity of 43.0 mS/cm and 57.2 mS/cm at a concentration of 0.65 M and 1.60 M, respectively, at 20 °C. A comparison of these two electrolytes is shown in **table 1.1**. As shown in **figure 1.1**, both the energy density and the power density of the GoldCap® capacitor improved significantly with a higher conductivity electrolyte.

In charging a double-layer capacitor, the charges are accumulated and separated at the interface between the electronic conducting electrodes and the ionic conducting electrolyte. The ionic charges that move to the interface from the electrolyte match the electronic charges from the electrodes. Therefore, the electrolyte functions not only as a media for ionic conduction but also as a source for ionic charge. Since the solubility of salt in nonaqueous solvent is not as high as that in water, the sufficient supply of the ionic charges becomes an issue that we cannot ignore. ARL is the first to recognize the importance of this aspect of the electrolyte for a capacitor **(7,8)**. When the ionic charge is considered, the energy density of the capacitor is no longer expressed as being based solely on the electrode materials, as shown by

$$E = \frac{1}{8} c_p V^2 \ , \tag{1}$$

where c_p is the specific capacitance of the electrode material and V is the operating voltage of the capacitor, which is limited by the decomposition potential of the electrolyte. The correct expression for the energy density should be **(7)**

$$E = \frac{1}{8} c_p V^2 \frac{1}{1 + \dfrac{c_p V}{4 a c_o F}} \ , \tag{2}$$

where c_o is the salt concentration of the electrolyte; F is the Faraday constant and equals 96,500 coulomb/M; and a, which is a unitless constant less than 1, represents the fraction of ions removed from the bulk of the electrolyte. Equation [2] clearly indicates that only when the ion concentration c_o is much greater than the charge capacity of the electrode $c_p V$ can the energy density of the double-layer capacitor be smaller than the usually conceived value as expressed in equation [1].

Table 1.1: Conductivity of the salt Et$_4$NBF$_4$ in PC and AN at 20 °C.

Solvent	Salt concentration (M)	σ (mS/cm)
PC	0.65	8.8
PC	0.86 (saturated)	12.4
AN	0.65	43.0
AN	1.68 (saturated)	57.2
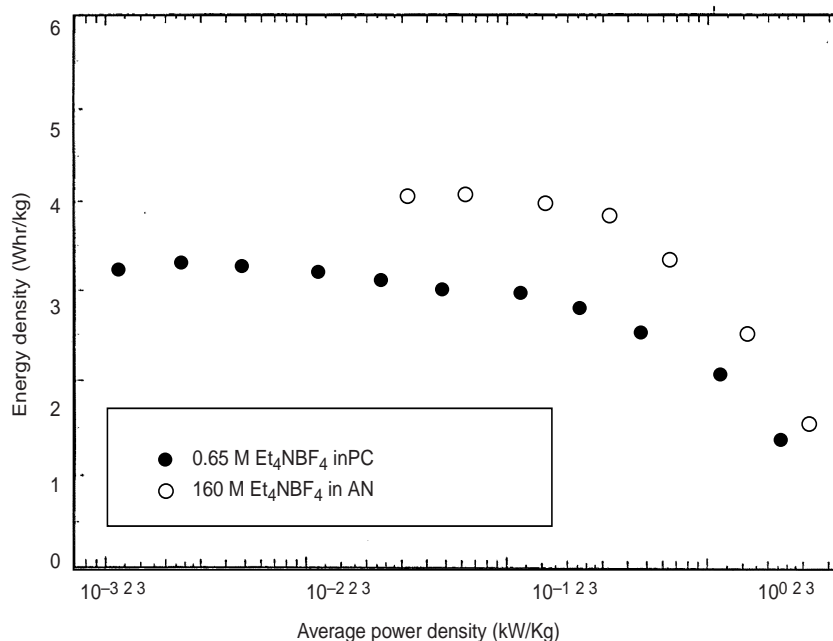
Figure 1.1: Comparisons of energy density vs. average power density for Panasonic capacitors containing 0.65 M Et$_4$NBF$_4$ in PC and 1.60 M Et$_4$NBF$_4$ in AN at 20°C.

Table 1.2 lists the maximum energy densities calculated using equation [2] for the state-of-the-art carbon-based double-layer capacitors in both aqueous and nonaqueous electrolytes. To achieve an energy density greater than 15 Wh/kg, as shown in the table, a nonaqueous electrolyte with a salt concentration greater than 1.5 M needs to be developed.

Based on the above consideration, it is important for electrolytes to have a high ion (or salt) concentration not only for high conductivity but also for high energy density. The high decomposition voltages of nonaqueous electrolytes allow a capacitor to operate at over 2.3 V as compared with 1.0 V for aqueous electrolytes. For energy density concerns, it is more advantageous to use nonaqueous electrolytes because the energy increases with the square of the voltage. However, the solubility of salt in a nonaqueous solvent is not as high as that in water; thus, having a sufficient supply of ionic charges becomes an issue that we cannot ignore.

The electrolytes also affect the capacitance of the electrode material as evidenced by a capacitance of 280 F/g observed for high surface area carbon in aqueous electrolyte and 120 F/g observed for the same carbon in nonaqueous electrolyte. Even in the same solvents, different values of capacitance are observed when the salts are different. As reported by Morita et al. (**9**),

Table 1.2: Energy limitations of the state-of-the-art carbon-based capacitors (calculated using $\alpha = 1/2$).

Capacitor system	Electrolyte	Maximum voltage (V)	c_p (F/g)	Energy density (Wh/kg) (electrode material only)	Energy density (Wh/kg) (electrode and electrolyte materials only)
Carbon/aqueous	5.26 M H_2SO_4	0.8	280	6.22	4.83
Carbon/aqueous	5.26 M KOH	0.8	280	6.22	5.11
Carbon/nonaqueous	0.75 M Et_4NBF_4/PC	3.0	120	37.5	9.69
Carbon/nonaqueous	1.5 M electrolyte	3.0	120	37.5	15

the discharge capacitance of the model capacitors is about 10 F/g in 0.5 M Bu_4NBF_4 in EC+γBL (50/50 by mol) but is about 16 F/g in 0.5 M Et_4NBF_4 in the same solvent mixtures. The difference can be attributed to the larger size of cation Bu_4N^+ than Et_4N^+.

1.2   Desired Properties and Controlling Parameters

From the above observation, we summarized the properties of the desired electrolyte and the controlling parameters in **table 1.3**.

1.3   State-of-the-Art Nonaqueous Electrolytes

The electrolyte used in state-of-the-art capacitors contains tetraethylammonium tetrafluoroborate (Et_4NBF_4) in propylene carbonate (PC) as described in patents by Matsushita **(6)** or in acetonitrile (AN) as described by Maxwell Technologies **(10)**. These electrolytes have their disadvantages.

The electrolyte of Et_4NBF_4 in PC exhibits a low salt concentration (saturated concentration is 0.86 M at room temperature) and low conductivity (8.8 mS/cm at 0.65 M at room temperature). This electrolyte is suitable for low-power applications such as memory protection but not for high-power applications.

For high-power applications, the electrolyte of Et_4NBF_4 in AN is used because of its high conductivity (about 50 mS/cm at 1.4 M at room temperature). The saturated salt concentration is about 1.68 M at room temperature, which is more concentrated than that in PC. The AN's lower oxidative stability and high vapor pressure make it less desirable for long life and high-temperature applications.

1.4   Recent Development

Better nonaqueous electrolytes for capacitors and Li-ion batteries are being intensively pursued. The selection of salt and solvent (or solvent mixture) is crucial in determining the overall electrolyte properties. However, in this project, we will concentrate mostly on the effect of salt. The recent development in the area of new salts for capacitors is reviewed below.

Table 1.3: Desired electrolyte properties and controlling parameters.

Desired properties	Parameters
$\sigma > 10$ mS/cm	solvents, salts (ε, η, μ, r_{ion} c_o), T
$\Delta V > 3$ V	solvents, salts, T, carbon
$c_o > 1.5$ M	solvents, salts, T
ΔT: –40 to 70 °C	solvents, salts, c_o, T_m
$c_p > 120$ F/g	solvents, salts, c_o, T, carbon

Key
σ: conductivity of electrolyte
ΔV: operating voltage window
c_o: salt concentration
T: temperature
ΔT: operating temperature range
c_p: specific capacitance of electrode material
ε permittivity of solvent
η: viscosity of solvent
μ: mobility of ions
r_{ion}: radius of ion
T_m: melting temperature of solvent.

Electrolytes Based on Quaternary Ammonium Salts

Ue et al. **(11–13)** reported recently that the solubility of the tetraalkyl ammonium salt in PC is substantially increased when asymmetry is introduced in the cation. For example, the solubility of Et_4NBF_4 salt with a symmetric cation in PC is less than 1 M at room temperature, while the solubility of Et_3MeNBF_4 with an asymmetric cation in PC is increased to 2 M at the same temperature.

Ue et al. **(11–13)** also reported that the solubility can be substantially increased by using a larger anion such as bis(trifluoromethylsulfonyl)imide (Im^{-1}) for a symmetric or an asymmetric quaternary ammonium cation.

The improvement in conductivity as a result of the increased solubility is only slight. At room temperature (25 °C), the conductivity of Et_4NBF_4 in PC is 12 mS/cm at a concentration ≤ 1 M, while the conductivities of 2-M Et_3MeNBF_4 or 2-M Et_4NIm in PC are 16 and 10 mS/cm, respectively.

The stability of Et_4NBF_4 in PC as compared with that of Et_3MeNBF_4 in PC is about the same. The limiting reduction and oxidation potentials for $Et_{4-n}Me_nNBF_4$, where n = 0 – 2, in PC are –3.0 and 3.60 V versus SCE (or 0.286 and 6.886 vs. Li^+/Li), respectively.

Electrolytes Based on Cyclic Aromatic Imidazolium Salts

McEwen et al. **(14)** recently described electrolytes containing salts based on aromatic imidazolium cations. Interestingly, many of these salts are liquids at room temperature.

Solubility as high as over 3.5 M is obtainable in PC with salts having aromatic ethylmethyl imidazolium cation (EMI$^+$).

To extend the liquid range, organic solvents are used with these salts. The conductivity of 2 M EMI PF$_6$ in PC is similar to that of 2 M Et$_3$MeNBF$_4$ in PC with a value of about 16 mS/cm at room temperature **(14, 15)**. The conductivity can reach as high as 60 mS/cm when AN is used as the solvent.

The reported electrochemical stability windows are 4.0 to 4.4 V for EMIIm and 1,2-dimethyl-3-propyl imidazolium (DMPIX)Im ionic liquids, respectively **(15–18)**. The electrochemical stability window of EMIPF$_6$ and EMIIm in organic solvents varies with the solvent. In PC, the stability window is about 4.0 V for both EMIPF$_6$ and EMIIm salts. We also noted that the limiting reduction potential is about –1.9 V versus Ag, or +1.1 V versus Li$^+$/Li.

1.5   Objective of This Development

Therefore, our main interest is in finding electrolytes with a high salt concentration (>1.5 M), high conductivity (>10 mS/cm in the temperature range from –20 °C to 50 °C), and large stability window (>3.0 V).

Comparing the quaternary ammonium salts with the cyclic aromatic imidazolium salts, the electrochemical stability window of the former is about 2.2 V larger than that of the latter. The above two salts provide similar conductivity for the same salt concentration in the same organic solvents. Furthermore, it was interesting to learn that the solubility of the quaternary ammonium salts can be significantly affected by the cation structure. In searching for electrolytes with a high conductivity, high solubility, and high operating window, we decided to look further into the class of quaternary ammonium salts, specifically those with variations in their cation structures.

We studied the commercially available quaternary ammonium salts with symmetric cation such as Et$_4$NBF$_4$ and Et$_4$NPF$_6$ in different solvent systems. The quaternary ammonium salts with asymmetric cation, which are not commercially available, were synthesized in our laboratory. We have synthesized a number of quaternary ammonium salts, especially with variations in cation symmetry. Some of these salts also had different anions. The synthesis methods and examples are detailed in **section 2**.

The electrolytes containing quaternary ammonium salts with asymmetric cation were studied mostly in EC-DMC (50:50) mixed solvents. The solubility, conductivity, electrochemical stability, and capacitance of the electrolytes containing these salts in EC-DMC are presented and discussed in **section 4**.

2. Synthesis of New Asymmetric Quaternary Ammonium Salts

2.1 Methods of Syntheses

The practice of the present syntheses will employ, unless otherwise indicated, conventional techniques of synthetic chemistry, electrochemistry, and battery/capacitor engineering that are within the skill of the art. Such techniques are explained fully or partially in the literature. See, for example, March's *Advanced Organic Chemistry* **(19)**, House's *Modern Synthetic Chemistry* **(20)**, Houben-Weyl's *Methoden der organischen Chemie* **(21)**, Hiers' text *Organic Synthesis* **(22)**, U.S. patent No. 4,892,944 to Mori et al. **(23)**, and Lindens' *Handbook of Batteries* **(24)**.

All chemicals used in the syntheses were used as received. The asymmetric ammonium salts were synthesized according to the following three methods.

1. Ue-Mori Approach: Convenient for anion-introduction.
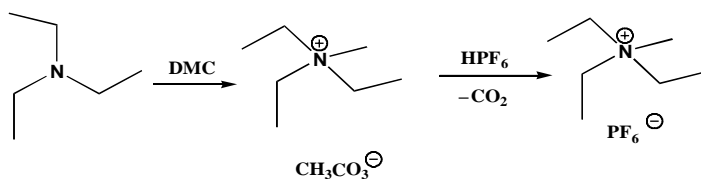
2. Modified Eschweiler-Clarke Procedure: Sterically crowded cation.
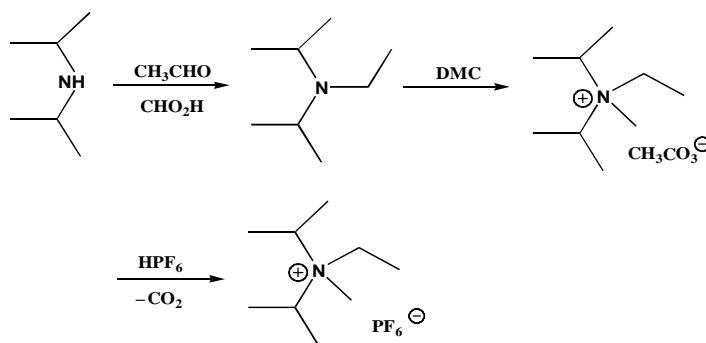
3. Controlled Exhaustive Alkylation: Very sterically hindered cation.
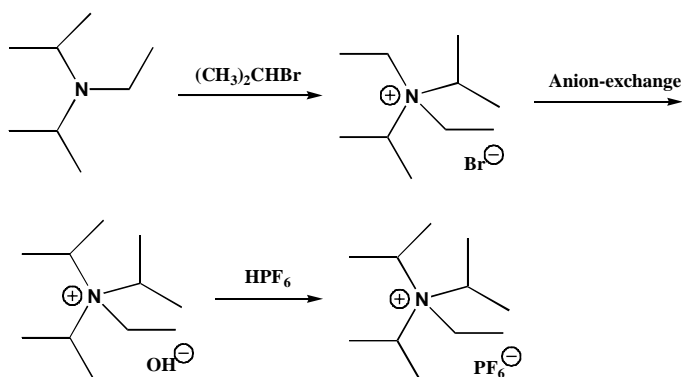
2.2 Examples

The steps of synthesizing the new asymmetric ammonium salts with variations in cation and anion are detailed in the following examples.

Example 1:
Synthesis of Ethylmethyldi(iso-propyl)ammonium
Hexafluorophosphate (EtMeiPr$_2$N$^+$PF$_6^-$)

In a 500-mL flask equipped with an addition funnel, a refluxing condenser and a stirrer were filled with 25.6 g of formic acid (0.5 mol, Aldrich, 95%) and 30.4 g of di(iso-propyl)amine (0.30 mol, Aldrich, 99.5%). During cooling and while being stirred, a 13.0-g acetaldehyde solution (~0.30 mol, Aldrich, 99%) was slowly added. After the solution became clear, the reaction mixture was brought to ~90 to 110 °C in an oil bath. A vigorous evolution of CO_2 began after 2 ~ 3 min., during which time the flask was removed from the bath from time to time until the evolution subsided. After 30 min., the reaction mixture stabilized and was kept in the oil bath at 100 °C for 8 hr.

After the solution cooled, 80 mL of 4.0 N HCl was added and the solution was evaporated until dry under reduced pressure. The remaining residue was dissolved in water and the organic phase was liberated by the addition of a 50-mL 9.0-N NaOH solution. The organic phase was separated and dried with anhydrous K_2CO_3. Distillation yielded ~32.0 g of ethyldi(iso-propyl)amine.

The above amine was mixed with 22.5 g of dimethylcarbonate (0.25 mol, Aldrich, 99%) in 100 mL of methanol. The mixture was then added to a Parr minireactor and the temperature was brought up to 130 °C for 5 hr. under vehement stirring. After the reaction, the product was transferred to a flask and evaporated under reduced pressure. The brownish residue, ethylmethyldi(iso-propyl)ammonium methylcarbonate (EtMeiPr$_2$NMeCO$_3$), weighs ~50.0 g.

EtMeiPr$_2$NMeCO$_3$ was dissolved in distilled water, and 60% hexafluorophosphoric acid (HPF$_6$) was added to this solution with precaution. After neutralization, the solution was evaporated under reduced pressure to remove water. The resultant crystal was repeatedly recrystallized from a hot methanol solution, and the final product obtained, EtMeiPr$_2$NPF$_6$, is fine needle crystal.

Example 2:
Synthesis of Ethylmethyldi(iso-propyl)ammonium
Bis(trifluoromethane sulfonyl)imide (EtMeiPr$_2$N$^+$Im$^-$)

We dissolved 40 g of lithium bis(trifluoromethane sulfonyl)imide (0.14 mol, 99%, 3M) in 200 mL of distilled water and passed it through a preprotonated cation exchange column of 4.5 equivalent capacity. The collected acid solution was once again passed through the regenerated cation exchange column to ensure quantitative conversion. The resultant aqueous solution of bis(trifluoromethane sulfonyl)imidic acid was condensed to ~2.0 M by evaporating the excess water.

The aqueous solution of bis(trifluoromethane sulfonyl)imidic acid was added to a solution of EtMeiPr$_2$NMeCO$_3$. After the neutralization, the solution was evaporated under reduced pressure to remove water. The resultant solid was repeatedly recrystallized from a hot methanol solution, and the final product obtained, EtMeiPr$_2$N$^+$Im$^-$, is fine needle crystal.

Example 3:
Synthesis of Ethylmethyldi(iso-propyl)ammonium
Triflate (EtMeiPr$_2$N$^+$Tf$^-$)

A triflic acid aqueous solution was prepared in a similar procedure as described in example 2, and it was then used to neutralize the solution of EtMeiPr$_2$NMeCO$_3$. After the neutralization, the solution was evaporated under reduced pressure to remove water. The resultant solid was repeatedly recrystallized from a hot methanol solution, and the final product obtained, EtMeiPr$_2$N$^+$Tf$^-$, is fine crystal.

Example 4:
Synthesis of Tri(iso-butyl)methyl ammonium Hexafluorophosphate (iBu$_3$MeN$^+$PF$_6^-$)

We charged 40.0 g of tri(iso-butyl)amine (0.21 mol, Aldrich, 98%) and 30.0 g of methyliodide (0.21 mol, Aldrich, 99%) in 200 mL of alcohol in a Parr minireactor. The reaction temperature was kept at 60 °C for 5 hr. before the reactor was opened. With the solvent evaporated under reduced pressure, the remaining solid residue was dissolved in water and passed through a strong base (in OH$^-$ form) anion exchange column with 4.0 equivalent capacity. The resultant basic solution was passed through the regenerated column again to ensure complete conversion.

After condensation, the basic solution was neutralized with HPF$_6$ and then the solution was evaporated under reduced pressure to remove water. The resultant solid was repeatedly recrystallized from a hot methanol solution, and the final product obtained, iBu$_3$MeN$^+$PF$_6^-$, is fine crystal.

Example 5:
Synthesis of Tri(iso-propyl)methylammonium Hexafluorophosphate (iPr$_3$MeN$^+$PF$_6^-$)

We mixed 40 g of di(isopropyl)amine (0.40 mol, Aldrich, 99.5%) in 100 mL of methanol with 51.2 g of formic acid (1.0 mol, Aldrich, 95%) in a 500-mL flask. While it was cooling and being stirred, we slowly added 33 g of formaldehyde solution (~0.40 mol, Aldrich, 37%). After the solution became clear, the reaction mixture was brought to ~90 to 110 °C in an oil bath. A vigorous evolution of CO$_2$ began after 2 ~ 3 min., during which time the flask was removed from the bath from time to time until the evolution subsided. After 30 min., the reaction mixture stabilized and was kept in the oil bath at 100 °C for 8 hr.

After the solution cooled, 100 mL of 4.0-N HCl was added and the solution was evaporated until dry under reduced pressure. The remaining residue was dissolved in water and the organic phase was liberated by the addition of 80 mL of 9.0-N NaOH solution. The organic phase was separated and dried with anhydrous K$_2$CO$_3$. Distillation yielded ~34.0 g of methyldi(iso-propyl)amine.

We slowly added 37.0 g of 2-bromopropane (0.30 mol, Aldrich, 99%) to the methyldi(iso-propyl)amine as obtained above. The reaction mixture was kept at room temperature overnight while being stirred. The crystal that formed was filtered and washed by methanol. The procedures for converting the crystal, which is methyltri(iso-propyl)ammnium bromide, into the corresponding hydroxide by anion exchange column, the subsequent neutralization with HPF$_6$, and the recrystallization in methanol is described in example 4. The resultant iPr$_3$MeNPF$_6$ is fine crystal.

Example 6:
Synthesis of Methyltripropylammonium Hexafluorophosphate ($Pr_3MeN^+PF_6^-$)

In a Parr minireactor, we charged 28.6 g of tripropylamine (0.2 mol, Aldrich, 99%) and 18.0 dimethylcarbonate (0.2 mol, Aldrich, 99%) in 200 mL of methanol. The reaction mixture was kept at 120 °C overnight, and the solvent and unreacted carbonate or amine were removed through evaporation under reduced pressure.

The brownish residue, $Pr_3MeN^+MeCO_3^-$, was dissolved in distilled water, and neutralization was carried out with HPF_6. The subsequent recrystallization procedure is described in example 3.

Example 7:
Synthesis of Ethyldimethylsulfonium Hexafluorophosphate ($EtMe_2S^+PF_6^-$)

We slowly added 15 g of ethylmethyl sulfide (0.20 mol, Aldrich, 99%) to 100 mL of a methyliodide solution in t-butyl methyl ether (0.20 mol, Aldrich, 2.0 M), and the reactants were kept at room temperature overnight. The crystalline precipitate was collected by filtration, washed by diethylether, and then dissolved in distilled water.

The procedures of converting the crystal, which is ethyldimethylsulfonium iodide, into the corresponding hydroxide by anion exchange column, the subsequent neutralization with HPF_6, and recrystallization in methanol are described in example 4. The resultant $EtMe_2SPF_6$ is fine crystal.

Example 8:
Synthesis of Triethylmethylammonium Hexafluorophosphate ($Et_3MeN^+PF_6^-$)

The synthesis of $Et_3MeN^+MeCO_3^-$ and its conversion into $Et_3MeN^+PF_6^-$ by means of anion exchange were conducted in a similar manner as described in example 6, except that an appropriate amount of triethylamine was used in place of tripropylamine. The resultant $Et_3MeN^+PF_6^-$ is fine crystal.

Example 9:
Synthesis of Triethylmethylammonium Bis(trifluoromethane sulfonyl)imide ($Et_3MeN^+Im^-$)

Using a 2.0-M aqueous solution of bis(trifluoromethane sulfonyl)imidic acid, whose preparation is described in example 2, an aqueous solution of $Et_3MeN^+MeCO_3^-$ was neutralized. After the neutralization, the solution was evaporated under reduced pressure to remove water. The resultant solid was repeatedly recrystallized from a hot methanol solution, and the final product, $Et_3MeN^+Im^-$, is fine needle crystal.

Example 10:
Synthesis of Triethylmethylammonium Triflate ($Et_3MeN^+Tf^-$)

Using a 2.0-M aqueous solution of triflic acid, whose preparation is described in example 3, an aqueous solution of $Et_3MeN^+MeCO_3^-$ was neutralized. After the neutralization, the solution was evaporated under reduced pressure to remove water. The resultant solid was repeatedly recrystallized from a hot methanol solution, and the final product, $Et_3MeN^+Tf^-$, is fine needle crystal.

Example 11:
Synthesis of Triethylmethylphosphonium Hexafluorophosphate ($Et_3MeP^+PF_6^-$)

The synthesis of $Et_3MeP^+MeCO_3^-$ and its conversion into $Et_3MeP^+PF_6^-$ by means of anion exchange were conducted in a similar manner as described in example 6, except that an appropriate amount of triethylphosphine was used in place of tripropylamine. The resultant $Et_3MeP^+PF_6^-$ is fine crystal.

Example 12:
Synthesis of Tributylmethylphosphonium Hexafluorophosphate ($Bu_3MeP^+PF_6^-$)

The synthesis of $Bu_3MeP^+MeCO_3^-$ and its conversion into $Bu_3MeP^+PF_6^-$ by means of anion exchange were conducted in a similar manner as described in example 6, except that an appropriate amount of tributylphosphine was used in place of tripropylamine. The resultant $Et_3MeP^+PF_6^-$ is fine crystal.

The onium salts that we have synthesized are summarized with their cations and anions listed in **table 2.1**.

2.3 Structure Identification

The structure of the new salts synthesized in this work was characterized using the nuclear magnetic resonance (NMR) method. **Figures 2.1 to 2.3** show the NMR spectra of some representative new salts synthesized in this work. In all cases, the chemical structure of the expected salt is confirmed by both the chemical shifts of proton nuclei signals as well as by the coupling (or splitting pattern) between the neighboring proton nuclei.

Table 2.1: The onium salts synthesized.

Figure 2.1: NMR spectra of tripropylmethylammonium cation.
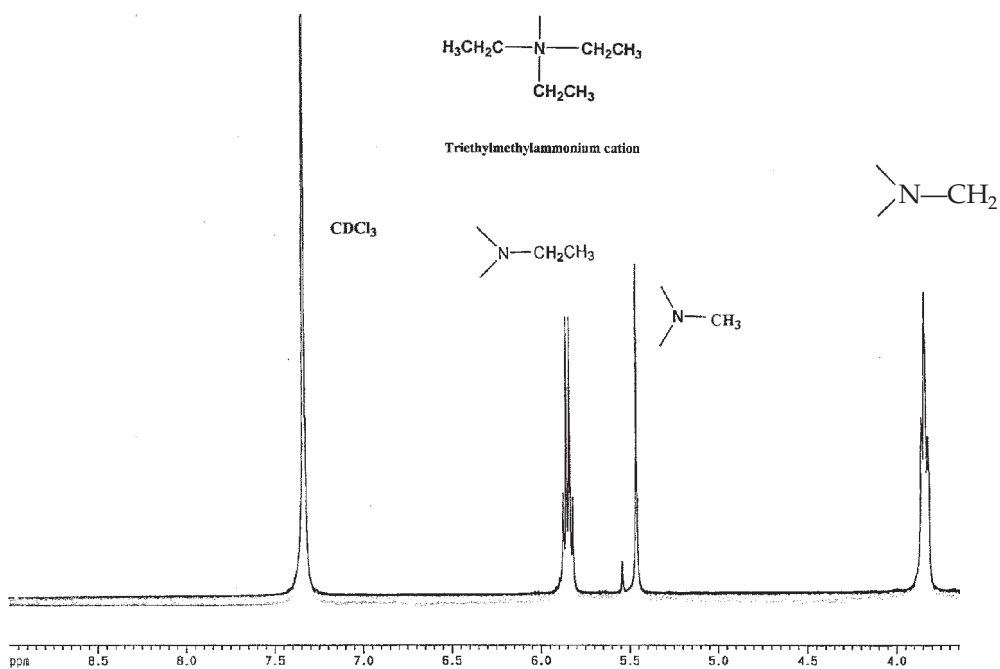
Figure 2.2: NMR spectra of triethylmethylammonium cation.

13
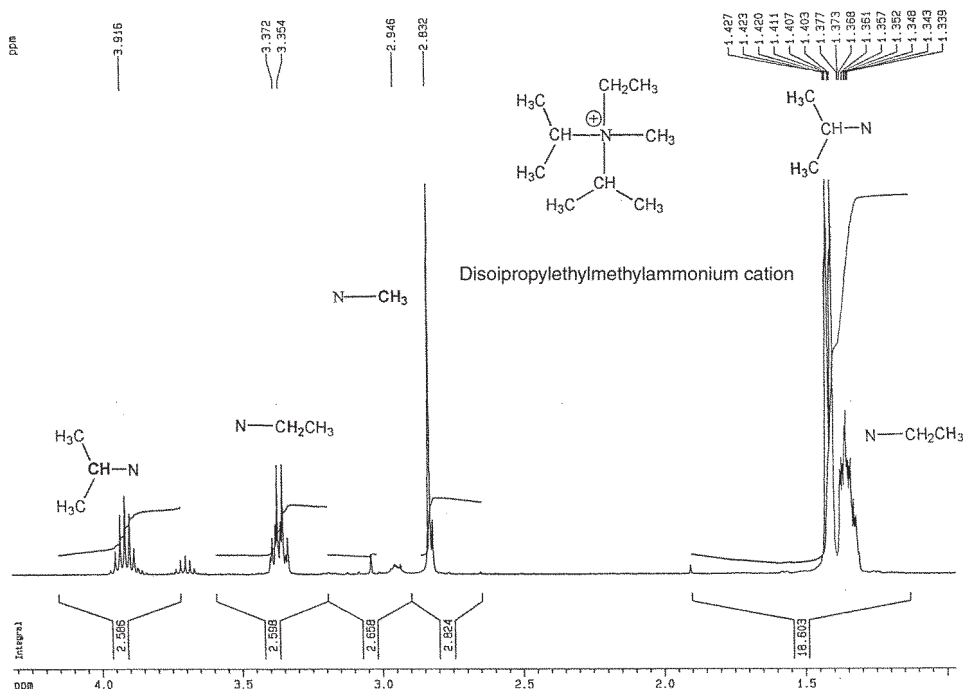
Figure 2.3: NMR spectra of diisopropylethylmethylammonium cation.

More importantly, the absence of other nuclear signals than the expected ones and the low, clean noise level also indicate the high purity of these salts. This corroborates the purity control achieved by repetitive recrystallization. For example, **figure 2.1** shows the NMR spectra of a **tripropylmethylammonium** cation. The chemical shifts for N-adjacent protons are typically between 3 ~ 4 ppm, with a distinct splitting pattern of CH_3–CH_2–CH_2–N as in propyl as well as a singular peak of CH_3–N. The integration under those peaks confirms the ratio of proton numbers corresponding to each alkyl group. This is a positive identification for the expected compound with high quality.

Figure 2.2 shows the NMR spectra of **triethylmethylammonium** cation. Likewise, CH_3CH_2–N and CH_3–N were identified by chemical shifts, peak integration, and the splitting pattern within ethyl. (An error in chemical shift labeling was made by the operator when the spectrum was plotted. The solvent used in this case is D_2O instead of CDCl, so the authentic chemical shift referred to the standard should be the labeling value minus 2.8.)

Figure 2.3 shows the NMR spectra of **diisopropylethylmethylammonium** cation. The conspicuous splitting pattern for isopropyl is obvious in the multiplets at 4.0 ppm, along with the clear CH_3–N and CH_3CH_2–N already seen in **figures 2.1 and 2.2**. The more complicated pattern in CH_3CH_2–N at 1.35 ppm is caused by the coupling effects from the sterically adjacent protons in isopropyl. This is expected because the bulky isopropyls crowd the space around the central N.

3. Experimental

3.1 Materials Preparation

The Et_4NPF_6 and the Et_4NBF_4 salts of 99% purity were obtained from Aldrich and used without further purification. The asymmetric quaternary ammonium salts were prepared using the methods described in **section 2** (Synthesis of New Asymmetric Quaternary Ammonium Salts). They were purified by triple recrystallization in methanol and then vacuum dried at 80 °C before use.

The solvents EC, DMC, and PC, were obtained from Grant Chemicals in electrochemical grade and further distilled before use. AN obtained from Aldrich was distilled before use. the ethylmethyl sulfone (EMSF) was synthesized in our laboratory. The physical properties of the solvents selected for our studies are listed in **table 3.1**. All solvents used in the fabrication of electrolytes were dried and redistilled.

Activated carbon (M series) from Osaka Gas was used without further treatment. The carbon electrode was prepared from 95 parts of activated carbon of various brands and 5 parts of Teflon as binder. The resultant mixture was dispersed thoroughly in an appropriate solvent. Then the solution was either evaporated to make an activated carbon-based paste, or directly coated onto an aluminum (Al) substrate by spraying. Typically the electrodes were cut into an area of ~100 cm^2, with a loading of ~2.8 mg/cm^2. The prepared electrodes were vigorously dried under vacuum.

We used different commercial separators, including Celgard® series films.

Table 3.1: Physical properties of selected solvents.

Solvent	ε	η (cP)	mp (°C)	bp (°C)	MW
Ethylene carbonate (EC)	95	1.85	35	244	88
Propylene carbonate (PC)	65	2.53	–49	242	102
Acetonitrile (AN)	36	0.343	–49	82	41
γ-Butyrolactone (BL)	42	1.73	–43	204	86
Glutaronitrile (GLN)	37	5.3	–29	286	94
N, N-dimethylformamide (DMF)	37	0.79	–61	153	73
Sulfolane (SL)	43	10	28	287	120
Diethyl carbonate (DEC)	2.82	0.748	–43	126	119
Dimethyl carbonate (DMC)	3.12	0.585	4.6	91	90
Ethylmethyl carbonate (EMC)	2.9	0.65	–55	107	104
Toluene (TL)	2.38	0.59	–95	110.6	92

Key
ε = dialectric constant
η = viscosity
mp = meling point
bp = boiling point
MW = molecular weight

3.2 Measurements

Melting Point (or Decomposition Temperatures) and Solubility

We used a Perkin-Elmer Differential Scanning Calorimetry (DSC) 7 to determine the melting point of the salts. The salt samples were sealed in aluminum sample pans under pure argon. Typically, we conducted the experiments under a helium atmosphere at a heating rate of 5 °C. We defined the point of the onset of melting as the melting point. We visually determined the solubility of the salts. To determine the solubility, a salt was slowly and continually dissolved in a specific amount of solvent until a solid residue remained that was stable against either shaking or shelving.

Electrical Conductivity

For electrolytic and molar conductivity measurements, samples of electrolytes were placed inside conductivity cells under argon. These cells were dip-type with cell constants near 0.1 cm^{-1} and sealable through a ground-glass opening on a filling tube connected to the cell body. Sample temperatures were kept constant during a measurement with a Tenney Engineering environmental chamber capable of both heating and cooling. We determined the solution's bulk resistance with impedance spectroscopy; we could then derive and conductivity from the cell geometry, which comprised a pair of parallel platinum electrodes. An HP 4284A precision LRC meter was used for the measurement. Densities of the electrolytes were measured with a Mettler-Toledo DA-110M density meter at room temperature.

Electrochemical Stability Window

The electrochemical stability window (ΔV) of the electrolyte was determined by measuring the limiting reduction (E_{red}) and oxidation potentials (E_{ox}) of the electrolyte against a glassy carbon working electrode with a diameter of 0.32 cm. These limiting potentials were measured by a linear sweep voltammetry technique using an EG&G 273 Potentiostat/Galvanostat controlled by a computer. A three-electrode configuration cell was employed, with glassy carbon as the working electrode, Li as the reference electrode, and platinum (Pt) as the counter electrode. Nickel (Ni) wire was also used as a reference electrode in some studies in which the electrolyte contained BF_4^- and PF_6^- anions. Large area Pt gauze was used as a counter electrode. The measurement was done in an argon-filled dry box. Typically, the scan rate was 5 mV/s, and $100\ \mu A/cm^2$ was used as the cutoff current density for the stability window limit. To evaluate E_{red} and E_{ox} of the electrolytes against porous activated carbon electrodes instead of the nonporous glassy carbon electrodes, we had to use a different method. This new method will be discussed in **section 4.3**.

Cell Testing

The assembled cell was subjected to a charge/discharge test on an EG&G 273 Potentiostat/Galvanostat. Typically, we used a charge/discharge rate of 1.0 mA/cm^2.

Table 3.2: Estimated ionic radii (*r*), molecular weight (MW), and single ion-limiting conductivity (λ_o).

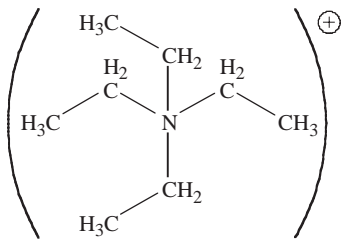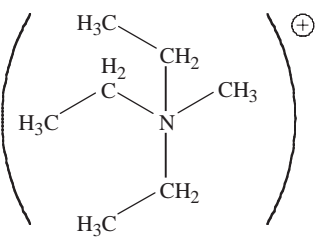| Ion	r (nm)	MW	λ_o in PC at 25 °C (S cm^2 mol^{-1})	λ_o in γ-BL at 25 °C (S cm^2 mol^{-1})
Li^+	0.076	6.94	8.43	13.99
Me_4N^+	0.283	74.147	14.50	21.52
Me_3EtN^+	0.298	88.174	14.14	20.77
$Me_2Et_2N^+$	0.313	102.201	13.90	20.18
$MeEt_3N^+$	0.327	116.228	13.68	19.70
Et_4N^+	0.343	103.255	13.50	19.32
Pr_4N^+	0.381	186.359	—	—
Bu_4N^+	0.415	242.467	9.09	14.03
ClO_4^-	0.237	99.449	18.93	28.45
BF_4^-	0.229	86.802	20.43	30.77
PF_6^-	0.254	144.964	19.86	26.70
AsF_6^-	0.260	188.912	17.58	25.92
$CF_3SO_3^-$	0.270	149.063	16.89	24.93
$(CF_3SO_2)_2N^-$	0.325	280.135	14.40	20.55
$C_4F_9SO_3^-$	0.339	299.087	13.03	18.66
BPh_4^-	0.419	319.232	8.52	11.52

4. Results and Discussion

4.1 Melting Point and Solubility

The increase in solubility as a result of a symmetry change in the cation structure is quite interesting. When the salt contains a cation with an asymmetric structure, we found that the solubility of the salt increases with increasing cation size (or cation molecular weight).

Results of the measurements on solubility and melting behavior of Et_4NPF_6 and Et_3MeNPF_6 salts are summarized in **table 4.1 (25)**, along with the structure and symmetricity of their cations. The solubility of Et_4NPF_6, in which the cation is symmetric, in EC-DMC was found to be 1.4 M at room temperature. The solubility of Et_3MeNPF_6, in which the cation is asymmetric, in EC-DMC was 2.2 M. For two salts that differ in their cations by only one methyl group in one constituent among four around the central nitrogen, the differences in solubility and melting behavior are strikingly large (1.4 M vs. 2.2 M). Since the most obvious change in going from the first salt to the second is from the symmetric cation Et_4N^+ to the unsymmetric cation Et_3MeN^+, it is reasonable to consider this symmetricity change as the primary cause for the differences in solubility and melting behavior of the two salts. We believe that by affecting the lattice energy of a salt, this change of cationic symmetricity causes the change in the salt's properties.

The lattice energy of an ionic solid comes primarily from the electrostatic attraction between the cations and the anions that form the solid. Its magnitude is inversely proportional to the average distance between the ions **(26)**. In the formation of the ionic salt Et_4NPF_6, the Et_4N^+ cations, owing to their symmetric shape, allow more efficient packing with PF_6^- anions than Et_3MeN^+ cations in the formation of Et_3MeNPF_6 salt. This packing results in a shorter average distance between the symmetric cations and the anions, giving Et_4NPF_6 a stronger lattice that is more difficult to break apart. When this breaking apart is attempted through thermal agitation, such as through heating in the DSC experiment, the stronger lattice of the salt manifests itself with a decomposition temperature that is 129 °C higher than the melting point of Et_3MeNPF_6 salt. When it is attempted through solvation by polar solvent molecules, such as

Table 4.1: Comparison of Et_4NPF_6 and Et_3MeNPF_6 salts.

Cation	Symmetric Et_4N^+	Asymmetric Et_3MeN^+
Cationic structure		
Salt	$(Et_4N)^+(PF_6)^-$	$(Et_3MeN)^+(PF_6)^-$
Solubility in 50:50 EC-DMC	1.4 M	2.2 M
Melting point	370 °C (decomposed)	240.9 °C

through dissolution in EC-DMC solvent, the stronger lattice again manifests itself with a solubility that is lower than that of Et_3MeNPF_6 by more than one-third in the units of molarity.

The same type of correlation between melting point and solubility has been observed for a series of tetraalkylammonium salts of the form $R'_1R''_3NPF_6$, where R' and R'' represent two different alkyl groups and their subscripts indicate that the cations have the same symmetricity **(25)**. As shown in **figure 4.1**, we observed that the melting point of the salt that contains an asymmetric cation decreases with an increase in the cation size **(27)**.

It is important to note that if Et_4NPF_6 salt was arranged in the above series according to the size of its cation, its melting point would be lower than that of Et_3MeNPF_6 salt. Instead, the lattice of Et_4NPF_6 salt, due to the symmetric shape of its Et_4N^+ cation, persists to a much higher temperature than that of Et_3MeNPF_6 salt. This indicates that, in addition to its size, the symmetry of an ion in a salt can affect the melting point or the lattice energy of a salt.

This effect, however, only occurs when the size difference is not too great. $EtMe_3NPF_6$ salt, for example, its cation being asymmetric but much smaller than Et_4N^+, decomposes at 389.1 °C, 19 °C higher than Et_4NPF_6 salt **(25).** When the asymmetric alkylammonium cation is combined with a larger anion such as Tf⁻ and Im⁻, the solubility in EC-DMC is increased to 3.1 and 2.7 M, respectively, versus 2.2 M for a smaller PF⁻ anion, as shown in **figure 4.2 (27)**.
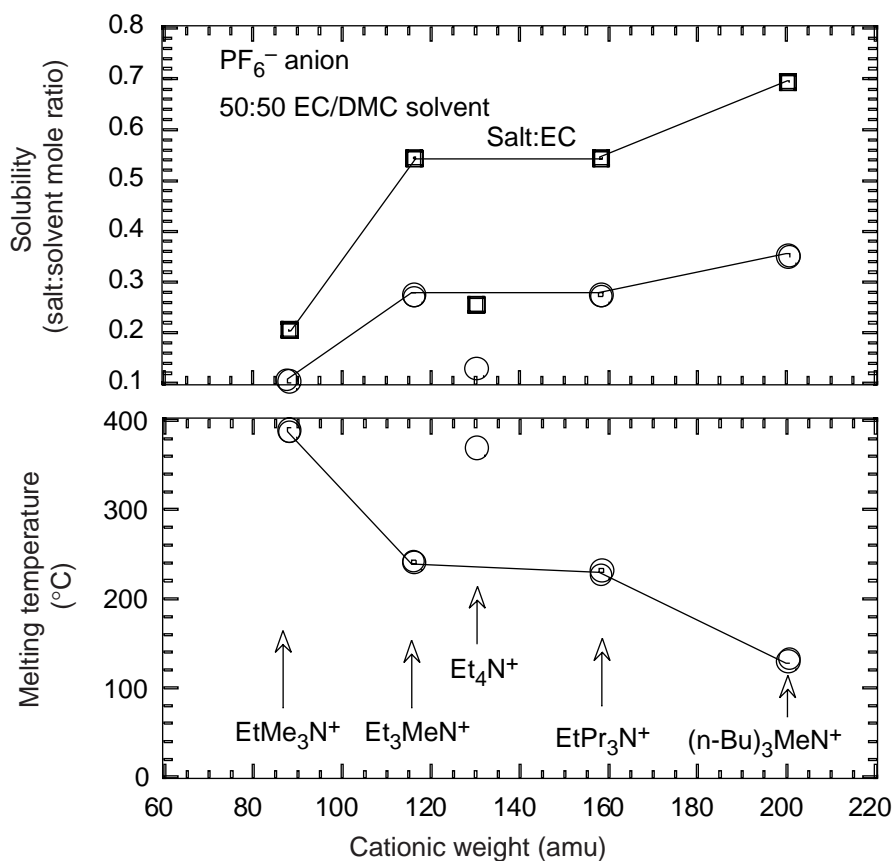

Figure 4.1: The correlation of melting point and solubility of asymmetry quaternary ammonium salts (in 50:50 EC-DMC) with variations in cation. Commercially available Et_4NPF_6 is used as a control.
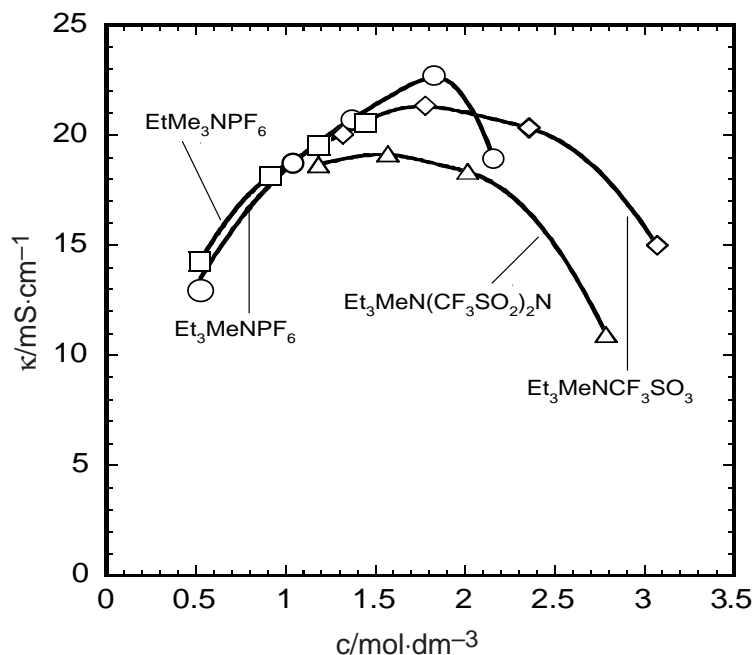
Figure 4.2: Room temperature electrolytic conductivities of EC-DMC (50:50 by wt.) solutions of asymmetric quaternary ammonium salts at different salt concentrations.

4.2 Conducitvity

Conductivity of Electrolytes Containing Et_4NBF_4 and Et_4NPF_6

The conductivities of the electrolytes containing the commercially available quaternary ammonium salt Et_4NBF_4 in various solvent systems at a concentration of 0.65 M and at the saturated concentration at room temperature are listed in **table 4.2**. The conductivities of these electrolytes as a function of temperature from –40 to 70 °C are shown in **figure 4.3.**

We note from **table 4.2.1** that both the conductivity and the salt concentration are higher for Et_4NBF_4 in AN, BL, and EC than in PC. Most notably, EC can dissolve Et_4NBF_4 up to 1.62 M and shows a conductivity of 19.12 mS/cm at room temperature. AN can dissolve 1.68 M Et_4NBF_4 and its conductivity reaches as high as 57.21 mS/cm. With the addition of EC to PC, both the conductivity and the salt concentration are increased. With the further addition of a low dielectric constant and low viscosity solvent such as DMC and TL, the conductivity is further increased but not the concentration.

The conductivity of Et_4NBF_4 in PC-EC as a function of concentration is shown in **figure 4.4**. The conductivity reaches its highest value of 13.8 mS/cm at a concentration of about 1.4 M.

Conductivity of Electrolytes Containing Asymmetric Quaternary Ammonium Salts

Results of conductivity measurements on the two sets of concentrated electrolytes are plotted in **figure 4.4** for Et_4NPF_6 (a) and Et_3MeNPF_6 (b) in 50:50 EC-DMC solvent. The solubility of Et_3MeNPF_6 salt is higher than that of Et_4NPF_6 salt in EC-DMC. However, their conductivity values are almost identical at the same concentrations. This is shown in a replotted, combined

Table 4.2: Conductivities of electrolytes containing Et_4NBF_4 in various solvent systems at a concentration of 0.65 M and at the saturated concentration.

Solvent system (ratio by wt.)	Saturated concentration (c), M	σ at c (M), mS/cm (20 °C)	σ_{max} at c (M/L), mS/cm (20 °C)
AN	1.68	43 @0.65 M/l	57.21 @1.68 M/L
AN/EC (15/85)	1.65	17.89 @0.65 M/L	27.26 @ 1.65 M/L
AN/EC (50/50)		35.47 @0.843 M/L	
AN/PC (15/85)	1.14	15.58 @0.65 M/L	20.51 @1.14 M/L
AN/PC (50/50)		27.93 @0.65 M/L	
AN/TL (50/50)	0.80	24.2 @0.61 M/L	25.8 @0.80 M/L
BL	1.18	13.4 @0.65 M/L	16.9 @1.18 M/L
BL/EC (50/50)		12.97 @0.65 M/L	
BL/TL (50/50)	0.49	9.04 @0.49 M/L	9.04 @0.49 M/L
PC	0.86	8.8 @0.65 M/L	12.44 @0.86 M/L
PC/EC (50/50)	1.311	11.03 @0.65 M/L	15.98 @1.311 M/L
PC/EC/AN (42.5/42.5/15)	1.37	16.78 @0.65 M/L	23.97 @1.37 M/L
PC/EC/DMC (42.5/42.5/15)	1.19	12.36 @0.65 M/L	17.46 @1.19 M/L
PC/EC/MF (42.5/42.5/15)	1.19	15.15 @0.65 M/L	20.39 @1.19 M/L
PC/EC/TL (42.5/42.5/15)		13.85 @0.65 M/kg	
AC	0.30	13.85 @0.30 M/L	13.85 @0.30 M/L
EC	1.625	19.12 @1.625 M/L[a]	19.12 @1.625 M/L[a]

Key
AC= acetone
AN = acetonitrile
BL = γ-butyrolactone
DMC = dimethyl carbonate
EC = ethylene carbonate
MF = methyl formate
PC = propylene carbonate
TL = toluene
[a]The lowest concentration at which both EC and the salt could be mutually dissolved is 1.24 M/L.

form in **figure 4.5** for ease of comparison. The measured conductivity values (dots) are connected by polynomial curves fitted to the values. Peak conductivities and the corresponding concentrations are evaluated from the polynomial curves and represented in the figures by the crosses and the curves connecting them. It can be seen from these figures that the conductivities of both electrolytes reach their maximum at different concentrations, depending on the type of salt and the temperature. The higher the temperature, the higher are the conductivities and the peak-conductivity concentrations. Furthermore, the peaks of Et_3MeNPF_6 electrolytes occur at concentrations substantially higher than those of Et_4NPF_6 electrolytes. On the other hand, the conductivity values of these two electrolytes almost overlap at all concentrations except those near and above peak-conductivity concentrations.
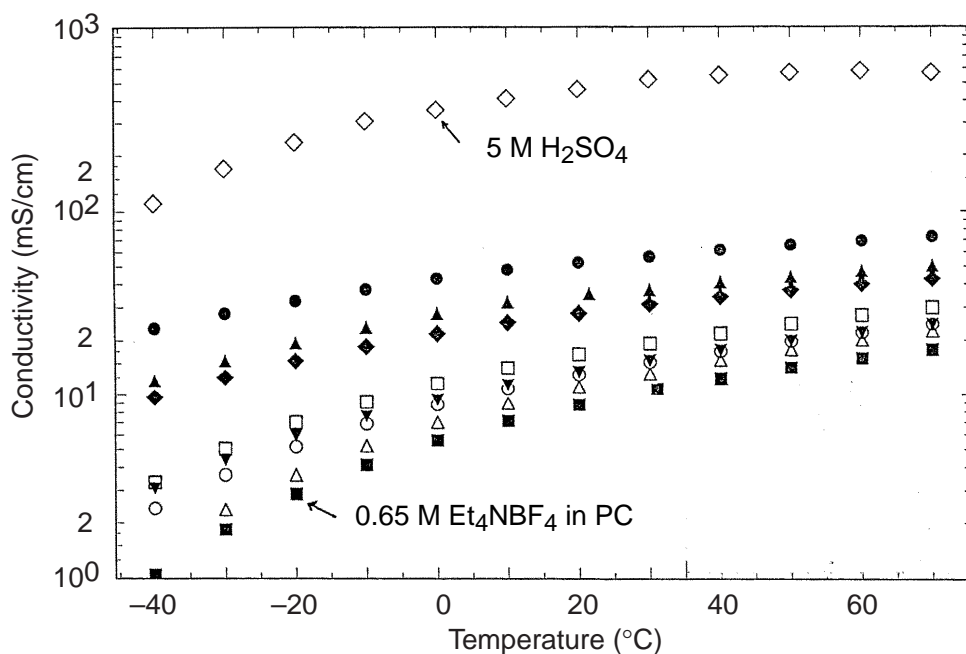
Figure 4.3: Conductivity vs. temperature from –40 to 70 °C for electrolytes containing 0.65 M Et$_4$NBF$_4$ in various solvent systems. (◇: 10 N H$_2$SO$_4$ solution, ●: 0.87 M Et$_4$NBF$_4$ in AN, ▲: 0.84 M Et$_4$NBF$_4$ in AN/EC (50/50 by wt.), ◆: 0.65 M Et$_4$NBF$_4$ in AN/PC, □: 0.65 M Et$_4$NBF$_4$ in EC/PC/AN (42.5/42.5/15), ▼: 0.65 M Et$_4$NBF$_4$ in BL, ○: 0.65 M Et$_4$NBF$_4$ in BL/EC (50/50), △: 0.65 M Et$_4$NBF$_4$ in EC/PC, ■: 0.65 M Et$_4$NBF$_4$ in PC).
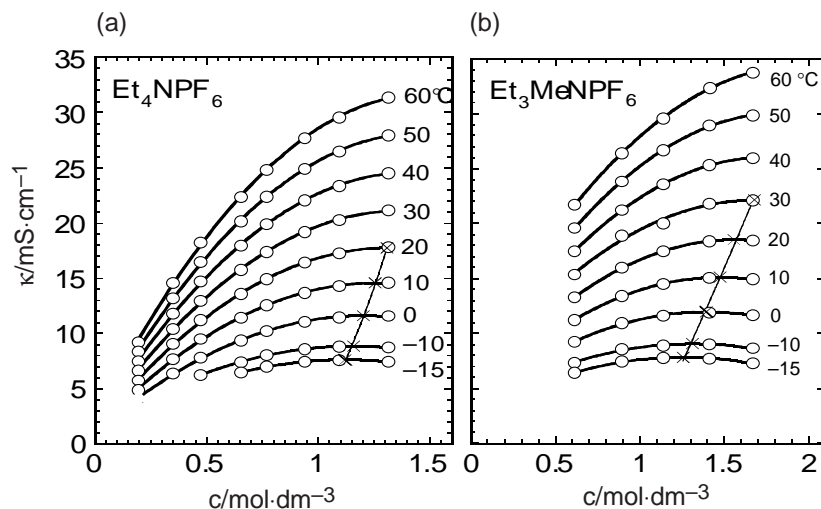
Figure 4.4: Change of electrolytic conductivity with salt concentration for electrolytes Et$_4$NPF$_6$ (a) and Et$_3$MeNPF$_6$ (b) in EC-DMC (50:50) at various temperatures.

The cation size of the quaternary ammonium salts has an impact on the conductivity of the electrolytes. We found that the conductivity decreases with increasing cation size. For example, the conductivity of 1.06 M (n-Bu)$_3$MeNPF$_6$ with a heavier cation in EC-DMC is lower than that of 1.04 M Et$_3$MeNPF$_6$ in EC-DMC, as shown in **figure 4.6 (28)**.

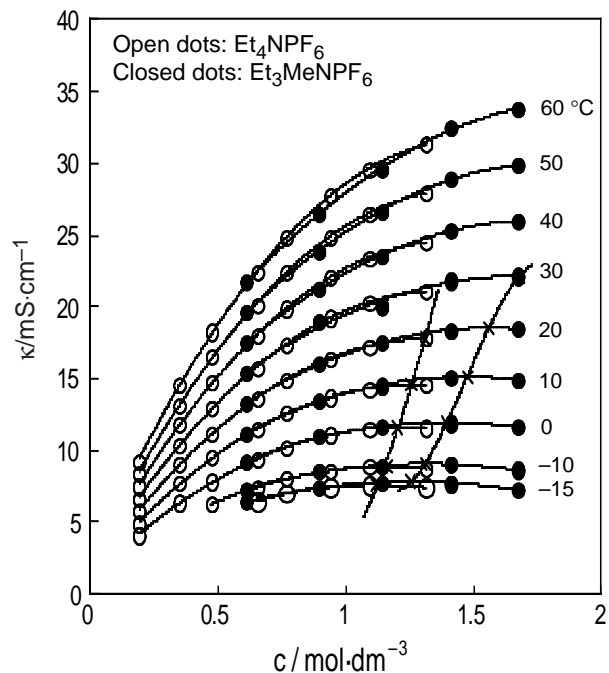**Figure 4.5: Electrolytic conductivity vs. salt concentration at temperatures from –15 to 60 ºC for Et$_4$NPF$_6$ and Et$_3$MeNPF$_6$ in EC-DMC (50:50).**
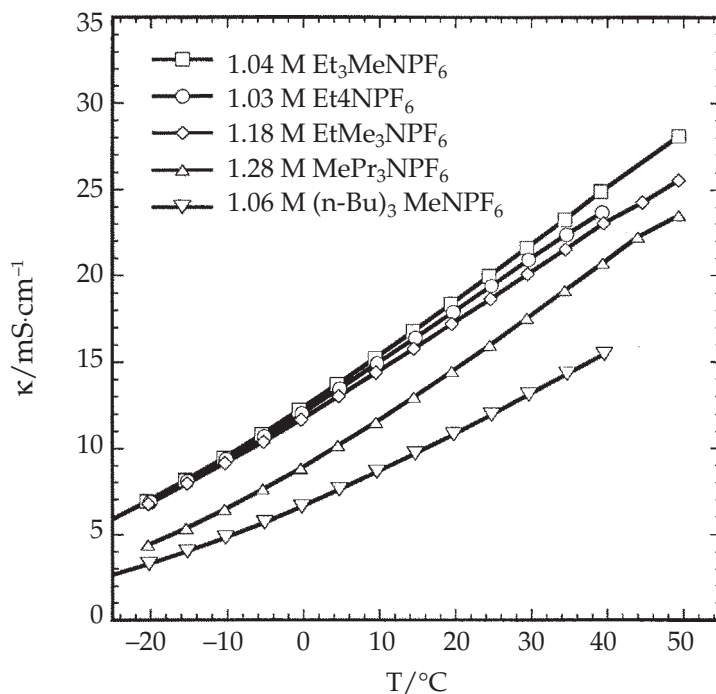

Figure 4.6: Change of conductivity with the size of the cations in tetraalkylammonium hexafluorophosphates for EC-DMC (50:50 by wt.) electrolytes containing such salts.

Limiting molar conductivities of the two salts in EC-DMC solvent at different temperatures are plotted in **figure 4.7**. These conductivities have been obtained by extrapolating to infinite dilution the molar conductivities of the two electrolytes measured with the two dilute electrolytes. In the temperature range measured, the values of Et_3MeNPF_6 salt are slightly larger than those of Et_4NPF_6 salt, and both show almost linear temperature dependence. **Figure 4.7** shows the limiting molar conductivities of these two electolytes **(28)** and those of $LiPF_6$ solutions of the same solvent. Compared to the latter, the densities of the two ammonium salt electrolytes are significantly smaller and very close to each other.

4.3 Electrochemical Stability

Electrochemical Stability versus Glassy Carbon

The limiting reduction potential E_{red} and the oxidation potential E_{ox} of each electrolyte were measured in a three-electrode cell using a linear sweep voltammetry technique. A glassy carbon rod and a platinum sheet were used as the working and the counter electrodes, respectively. A piece of lithium metal was used as a reference electrode.

Results of the electrochemical stability measurements with linear sweep voltammetry with glassy carbon working electrodes are shown in **figure 4.8** for the two electrolytes in the same EC-DMC solvent but with 1 M salts of Et_4NPF_6 and Et_3MeNPF_6, respectively. It can be seen that both salts have stability windows more than 6.5 V wide. Close inspection of the results shows that the two salts have almost identical reductive stabilities in EC-DMC solvent on glassy carbon. The stability window of 1 M Et_4NPF_6 in AN is also included for comparison. The oxidative stability of this electrolyte is more than 1 V lower than that of the electrolyte containing EC-DMC solvent.

As shown in **figure 4.9**, the limiting reduction potentials of various quaternary ammonium salts containing either symmetric or asymmetric cations such as Et_4N^+, Me_3EtN^+,
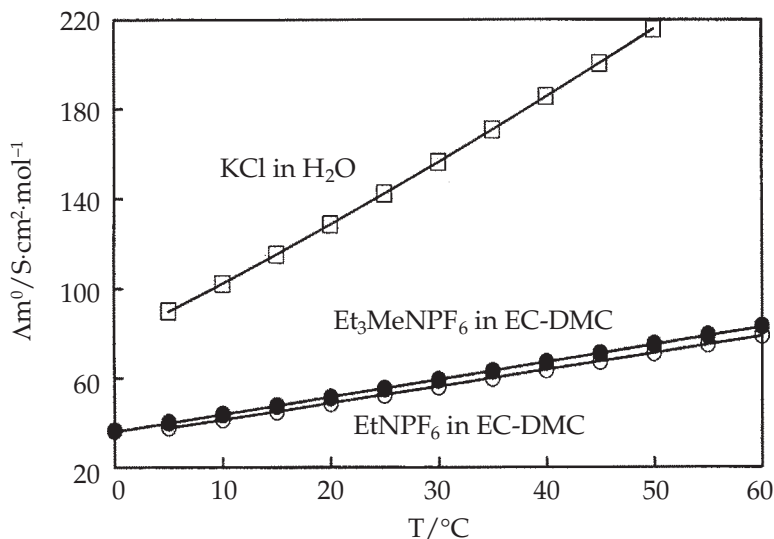
Figure 4.7: Limiting molar conductivities of two electrolytes, Et_3MeNPF_6 and Et_4NPF_6, respectively, in EC-DMC (50:50) at different temperatures. Those of KCl in water are plotted for reference and comparison.
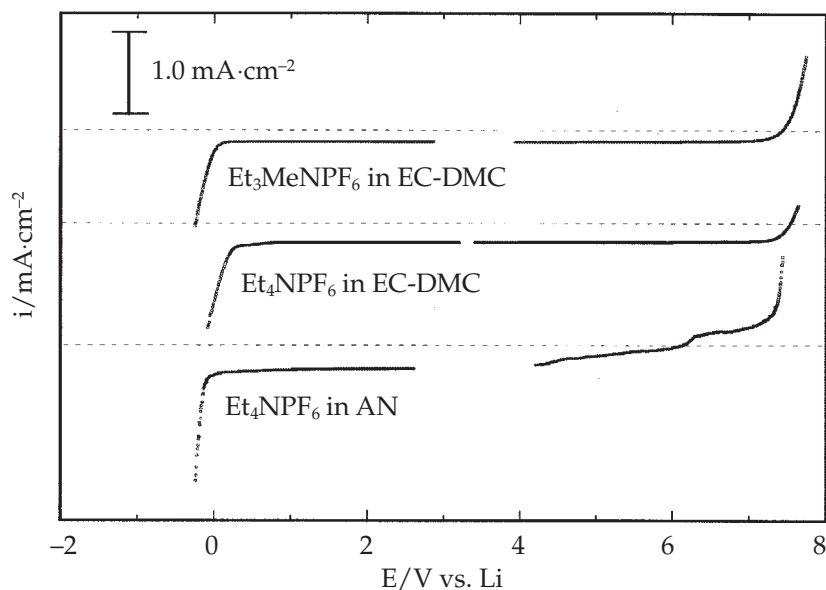
Figure 4.8: Linear sweep voltammograms for electrolyte solutions of Et$_4$NPF$_6$ and Et$_3$MeNPF$_6$ in EC-DMC (50:50) on glassy carbon. That for Et$_4$NPF$_6$ in AN is plotted for comparison.
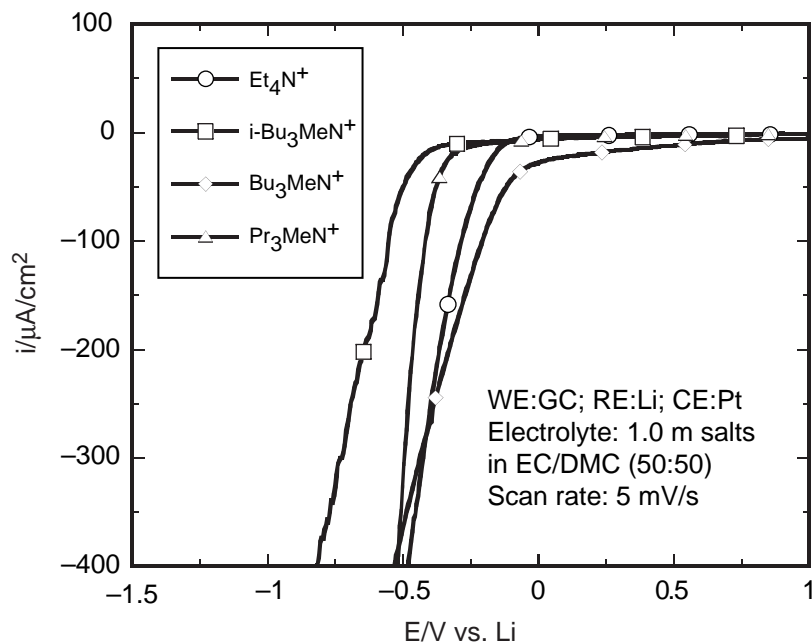
Figure 4.9: Comparison of cathodic stability of various onium cations synthesized.

Et$_3$MeN$^+$, Pr$_3$MeN$^+$, Bu$_3$MeN$^+$ in EC-DMC with PF$_6^-$ anion exhibited similar values at about –0.5 V versus Li$^+$/Li (the voltage value at which the current reaches 500 µA/cm^2) at a scan rate of 5 mV/s **(27).** These results indicate that the solvent also plays a role in the reductive stability of the electrolyte. When the asymmetric quaternary ammonium cation contains a more spatially hindered group such as i-Bu$_3$MeN$^+$, the limiting reduction potentials were further extended from –0.5 to –1.0 V versus Li$^+$/Li as shown in **figure 4.10 (27)**.
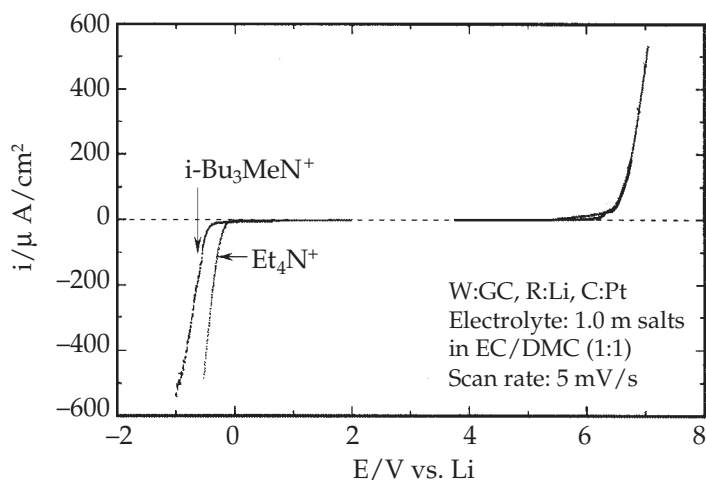
Figure 4.10: The total electrochemical stability window of a conventional ammonium salt and a new ammonium salt with steric hindrance.

The E_{ox} values of the electrolytes containing quaternary ammonium salts were independent of the cations. We found, however, that they are dictated by the stability of anions or solvents. As shown in **figure 4.11**, the E_{ox} of PF_6^- anion is about 6.5 V versus Li^+/Li, which is about 1 V higher than that of trifluoromethylsulfonate ($CF_3SO_3^-$ Tf^-) anion and bis(trifluoromethylsulfonyl)imide (($CF_3SO_2)_2$ N^-, Im) anion.

Electrochemical Stability versus Porous Activated Carbon Electrodes

The electrochemical stability window of an electrolyte is usually determined by the limiting reduction and oxidation potentials of the electrolyte against a glassy carbon working electrode using a linear sweep voltammetry technique. The stability window values obtained by this method cannot be used to determine the safe operating voltage of a capacitor. Part of the reason for this is that the surface area of the glassy carbon is too low to produce a level of current that is high enough to tell that the instability has already occurred before the catastrophic decomposition. Furthermore, the surface properties of each activated carbon are different from that of a glassy carbon.

Using a porous electrode made of an activated carbon instead of a glassy carbon electrode presents a practical problem **(27, 30)**. Instead of zero background current, we have observed a large and symmetric current (i.e., $Q_A = Q_C = Q_{NF}$, where Q_{NF} is charge due to the reversible capacitive current or a non-Faradaic current) when the voltage scan is within the stability limits (see **fig. 4.12**). When the voltage scan went beyond the stability limits, the charge measured would include not only Q_{NF} but also Q_F, which is the charge due to the irreversible electrolyte decomposition or a Faradaic current. Furthermore, we observed that the current measured did not increase but decreased as a result of the instability. This is because the Faradaic reaction between the electrolyte and the electrode reduced the available surface area of the activated carbon electrode before the catastrophic reactions occurred. Therefore, a new method to quantify the stability limits is needed. Instead of scanning the potential all the way to the limiting
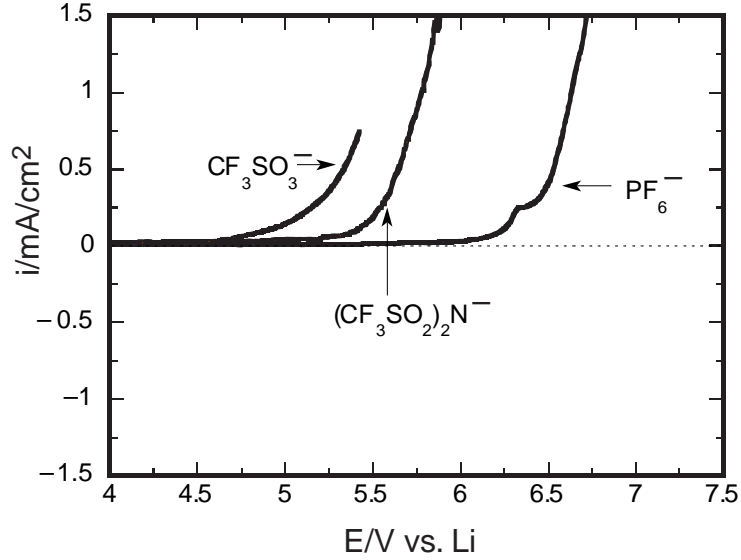
Figure 4.11: Comparison of anodic stability of various anions.
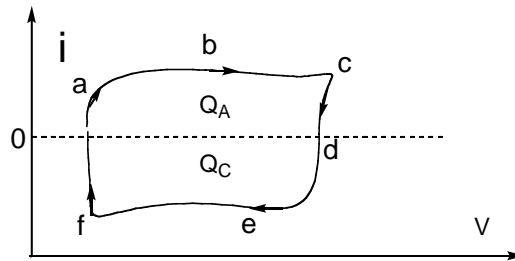
$$R = \frac{|Q_F|}{|Q_{NF}|} = \frac{|Q_A|}{|Q_C|} - 1.0$$

Figure 4.12: The CV curve of an electrolyte against a porous activated carbon electrode. Instead of a zero background current, a large background current was observed. Within the stability window, there is only non-Faradaic charge Q_{NF}, (or capacitive charging current) but no Faradaic charge Q_F. The Q_F-to-Q_{NF} ratio, R, should be zero when the voltages are within the stability window.

potentials, we successively scanned the potential from a small value toward the limiting potentials. At each voltage scan, we use the ratio R, which is defined as

$$R = \frac{|Q_F|}{|Q_{NF}|} = \frac{|Q_A|}{|Q_C|} - 1.0 \ ,$$

to judge whether the voltage is still within the stability limits. An R thus defined will give the ideal value 0 as long as the Faradaic irreversible process is negligible, and will be greater than 0 in both the anodic or cathodic territories once the decomposition of the electrolyte starts occurring to a discernible extent. If a series of scans is done with successively increasing (or

decreasing) voltage limits, then *R* of each scan is plotted versus the potential limit of that scan. This plot should accurately reflect the onset potential of any Faradaic process indicated by the deviation of *R* from the ideal value 0, as schematically depicted in **figure 4.13**.

Figure 4.14 shows the result of actually applying the procedure depicted by **figure 4.13** to an electrolytic solution of 1.0 M Et_4NPF_6 in 50:50 EC-DMC. By choosing an arbitrary reversibility limit of *R* = 0.1 (i.e., the decomposition of electrolyte accounts for ~ 10% of the total charge infused into the capacitor), the electrochemical stability window of this electrolyte, which is now well defined, would be 2.71 V, with reduction and oxidation potentials at 1.81 V and 4.52 V versus the Li reference electrode, respectively. At potentials lower than 1.0 V and higher than 5.0 V versus Li/Li$^+$, the electrolyte undergoes substantial decomposition, giving the maximum stability window of ~4.0 V. This value corresponds well with the actual working voltage limit of nonaqueous supercapacitors.

Several other nonaqueous electrolyte systems were evaluated by this new method using an asymmetrical tetraalkylammonium salt ($Et_3MeN^+PF_6^-$) as electrolyte solute, and the results are summarized in **figure 4.15**. With some slight variations, their stability windows all lay in the range of ~1.5 V to ~4.5 V versus Li, with the exception of the ethylmethyl sulfone-containing electrolyte. This electrolyte is especially resistant to reduction and thus yields a stability window as wide as 3.64 V. All these stability windows are obviously narrower than measured on nonporous electrodes and would more accurately reflect the real stability window in actual capacitor devices. Of special interest is the difference in the stability window of $Et_3MeN^+PF_6^-$ and $Et_4N^+PF_6^-$ in the same solvent 50:50 EC-DMC (compare **fig. 4.14 and 4.15**). The symmetrical salt cation (Et_4N^+) shows a little more cathodic stability than its asymmetrical counterpart (Et_3MeN^+), while this difference is hardly detectable on the glassy carbon working electrode. We attribute this different ability to resist cation reduction to the shielding effect of the central cation by its alkyl substituents, which will be discussed in more detail in our future publication **(27)**.
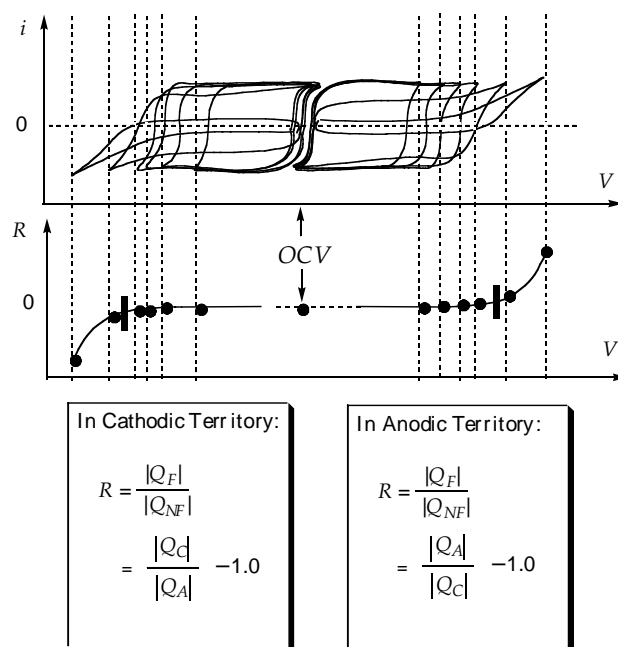
Figure 4.13: New method for the quantification of electrolyte stability range on activated carbon.
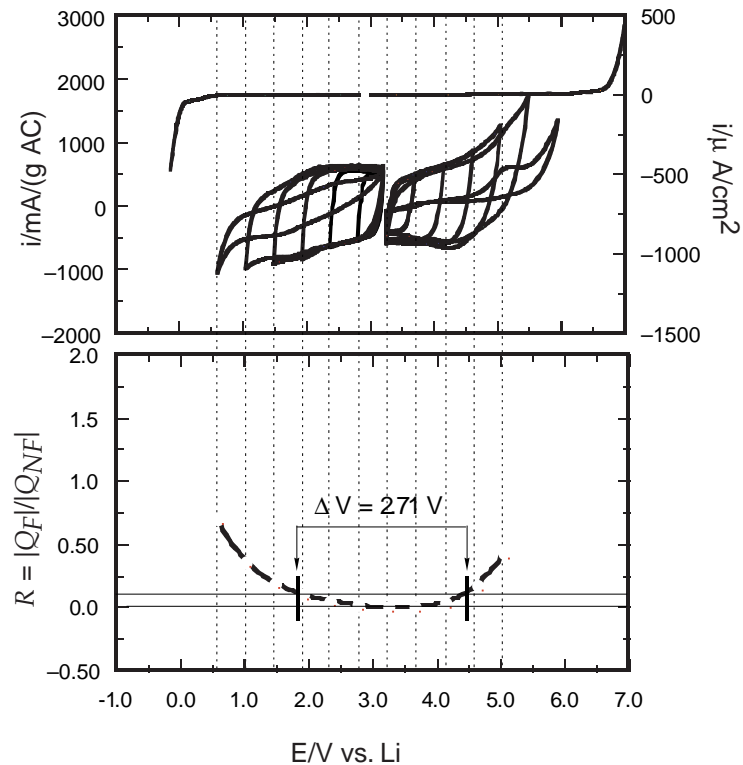
Figure 4.14: The electrochemical stability range of electrolyte 1.0 M Et$_4$NPF$_6$ in EC-DMC (50:50) according to the new quantification.
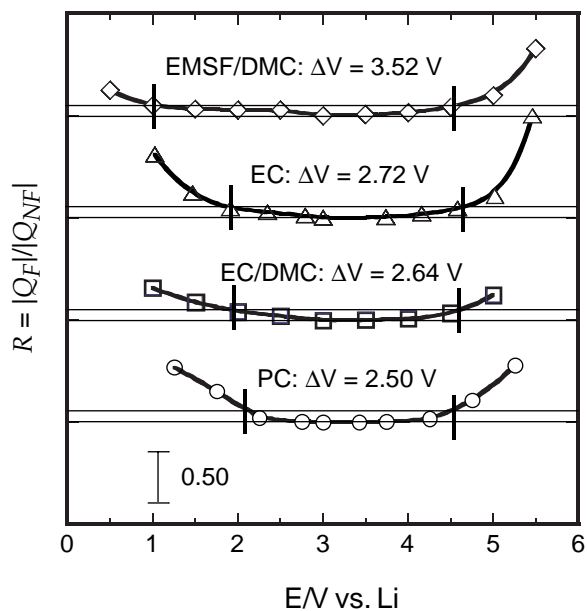

Figure 4.15: The electrochemical stability window of several electrolytes containing 1.0 M Et$_3$MeNPF$_6$ in solvent systems such as PC, EC-DMC, EC, and EMSF-DMC determined by the new quantification method.

4.4 Capacitance

Capacitance values of carbon materials in electrolytes are insensitive to the dielectric constant of the solvent used. We found that the capacitance values of capacitors made with activated carbon electrodes in 0.65 M Et_4NBF_4 in PC, AN, and MF/AN were 6.94, 6.91, and 6.72 F, respectively. The dielectric constants of PC, AN, and MF/AN are 64.4, 36.0, and 22.5, respectively. This result is consistent with the recent studies reported by McEwen et al. **(29)**. They found that the specific capacitance values of carbon in 2 M ethylmethyl imidazolium hexafluorophosphate ($EMIPF_6$) in EC, PC, DMC, EMC, EC-DMC (1:1 v/v), and PC-EMC (1:1 v/v) are 123, 127, 126, 123, 129, and 129 F/g, respectively. As we note in **table 3.1**, the dielectric constants of EC and PC are 95 and 65, respectively, while that of DMC and EMC are 3.12 and 2.9, respectively.

However, the capacitance measured was sensitive to the molecular size of the salt used. For example, capacitance values of 0.666 and 0.799 F were measured in electrolytes of 0.65 M Et_4NBF_4/PC and 0.65 M Et_4NSCN/PC, respectively. The larger capacitance value measured with the SCN^- anion is attributed to its smaller ion size.

The double-layer capacitance that we have measured was about 130 to 150 F/g for an Osaku Gas M30 activated carbon in quaternary ammonium salts containing cation with different structures (or alkyl groups) in EC-DMC. We have not observed significant capacitance value changes as a result of changes in cation size of the asymmetric quaternary ammonium cation in the salt. Since the capacitance measured is a reflection of the effect of both cation and anion, the impact from the cation alone may not be sufficient to show the difference. However, we should note a recent report by Morita et al. **(9)**. Their model capacitors showed a value of 10 F/g in 0.5 M Bu_4NBF_4 in EC-γBL, while a value of 16 F/g was shown in 0.5 M Et_4NBF_4 in EC-γBL.

4.5 A Comparison of ARL Electrolytes With the State-of-the-Art Electrolytes

The electrolytes that we developed under this project that exhibited the best combination of salt concentration and electrochemical stability window are listed in **table 4.3**. The state-of-the-art electrolytes are also listed for comparison. The energy density calculated with equation [2] reaches as high as 20 Wh/kg counting only the electrode material and the electrolyte, where the salt concentration is 1.5 M/kg and the operating voltage is 3.5 V. We did not have sufficient time for further search of solvents for our new salts in this project. However, the identification of EMSF as a more stable solvent is an important discovery. This clearly suggests that more effort is needed in the area of solvents. A recent report by Hirahara et al. **(31)** confirms our belief that the electrode material is also critical in determining the operating voltage and the stability of the electrochemical capacitor at elevated temperatures.

4.6 Cell Performance

After vigorous drying, the electrodes and the separator were vacuum-soaked with an electrolyte containing Et_3MeNPF_6 in EC-DMC and were assembled as an experimental capacitor cell. **Figure 4.16** shows the voltage profile for galvanostatic charging/discharging of such a capacitor that comprises the electrolytes that were developed in this project. The charge/

discharge were carried at different operating voltages, and eventually the voltage was deliberately brought over the decomposition potential of the electrolytes. While Panasonic's GoldCap®, capacitor burst the safety valve at ~4.0 V charging, the electrolytes developed in this project operated well at 4.0 V, and did not burst even at 5.0 V in a cell with the same safety valve.

We planned to test prototype capacitors of a size of 100 F/2.3 V from Maxwell Technologies with our electrolytes. Our specific interests are stability of the capacitor under voltage bias from 2.3 to 3.0 V at elevated temperatures of about 40 to 60 °C and the performance of the capacitors at low temperatures of about –10 to –30 °C. However, the amount of purified electrolyte and the time to complete the above tests were beyond the scope of the present project.

Table 4.3: A comparison of ARL electrolytes with the state-of-the-art electrolytes.

ARL electrolyte

Salt	Solvent	C (M/kg)	c_p (F/g)	σ (mS/cm)	ΔV (V): GC	ΔV (V): AC	ε (Wh/kg)
Et_3MeNPF_6	EMSF-DMC	1.5	120	—	—	3.50	20.33
Pr_3MeNPF_6	EC-DMC	1.28	120	14	6.78	3.04	15.55
Et_3MeNPF_6	EC-DMC	1.5	120	19	6.54	2.50	12.79

State-of-the-art electrolyte

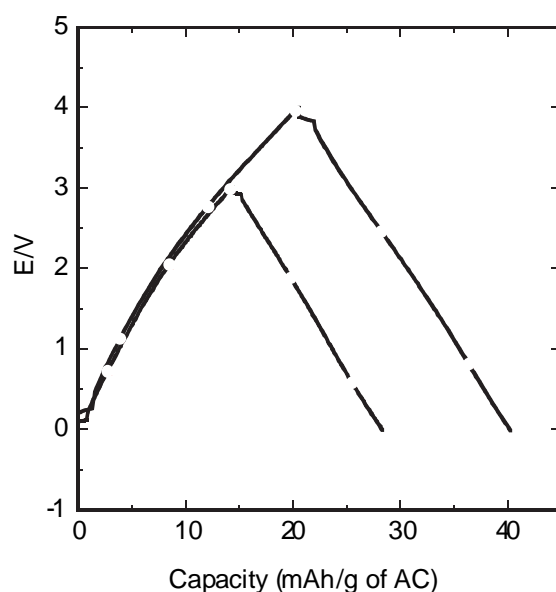| Salt	Solvent	C (M/kg)	c_p (F/g)	σ (mS/cm)	ΔV (V): GC	ΔV (V): AC	ε (Wh/kg)
Et_4NBF_4	PC	0.72 (0.75 M)	120	10	6.15[a]	2.9[a]	9.99
Et_4NBF_4	AN	3.85 (1.68 M)	120	57	3.5–4.0[a]	2.0[a]	12.60
$EMIPF_6$	PC	2.62 (2 M)	120	16	4.5[a]	2.0[a]	11.30

[a]Estimated value.

Figure 4.16: Charge/discharge voltage profile of a Panasonic GoldCap®, capacitor in original electrolyte (lower curve) and in 1.0 M Et_3MeNPF_6 in EC-DMC (upper curve).

5. Conclusions and Future Perspective

Nonaqueous electrolytes were formulated and evaluated for double-layer capacitors. For a commercially available salt, Et_4NBF_4, the more promising solvents were a blend of ethylene carbonate (high dielectric constant) and a second low-viscosity liquid. Several formulations were prepared with a conductivity over 15 mS/cm, a salt concentration over 1 M (1.4 to 1.6 M), and an electrochemical stability window of over 6.5 V against a glassy carbon electrode.

With the change in cation from symmetric ones to asymmetric ones in quaternary ammonium salts, we have shown that a significant change in solubility occurs in EC-DMC that ranges from 1.4 M to 2.2 M. A conductivity peak of the electrolyte is shifted to a higher salt concentration for the asymmetric cation. A conductivity value as high as 22 mS/cm has been achieved. The ion size of the cation affects the solubility and the conductivity of the electrolytes containing these salts. Salts containing a spatially hindered cation, $i\text{-}Bu_3MeNPF_6$, exhibited a limiting reduction potential 0.5 V larger than other asymmetric cations.

Since the electrochemical stability window values obtained for electrolytes normally use a glassy carbon electrode as a working electrode, the values obtained by such a method—for example, 6.5 V—are often much larger than the real operating voltages—for example, 2.3 to 3.0 V. To obtain a realistic value of the stability window for a practical carbon material, the traditional method of using an arbitrary current value as a limit to determine the voltage limit does not work for the high surface area carbon materials. A new method that uses charge, or an integration of current, instead of using current directly to detect the instability limit gave us values that more realistically reflect the true stability window. Using the new method and a new salt, we learned that the stability window of the electrolyte varies with solvent too. Our study was not exhaustive; however, our discovery that the sulfone-based solvent achieved a stability window as high as 3.5 V is important.

The high salt concentration together with the large operating voltage window lead to high energy density and high power density capacitors. Demonstration of the new electrolytes in practical capacitors is certainly needed. Looking forward, more effort in the study of a solvent for low-temperature performance is needed. For high-temperature stability and high-voltage operations, studies of both solvent and carbon electrode materials are needed. For the next phase, the participation of a capacitor manufacturer for carbon electrode fabrication and capacitor assembly and a chemical company for electrolyte preparation and purification will speed up the development of high-energy and high-power electrochemical capacitors.

References

1. T. R. Jow, "High Energy Density Capacitors Based on Electrostatic Energy," *Proceedings of the 2nd International Seminar on Double Layer Capacitors and Similar Energy Storage Devices*, Deerfield Beach, FL (December 7–9, 1992).

2. T. R. Jow and J. P. Zheng, "Electrochemical Capacitors Based on Amorphous Ruthenium Oxide," *Proceeding of the 4th International Seminar on Double Layer Capacitors and Similar Energy Storage Devices*, Deerfield Beach, FL (December 12–14, 1994).

3. J. P. Zheng and T. R. Jow, "A New Charge Storage Mechanism for Electrochemical Capacitors," *J. Electrochem. Soc.*, **142** (1), L6 (1995).

4. J. P. Zheng and T. R. Jow, "High Energy and High Power Density Electrochemical Capacitors," *J. Power Sources*, **62**/2, 155 (1996).

5. T. R. Jow and J. P. Zheng, "Electrochemical Capacitors Using Hydrous Ruthenium Oxide and Hydrogen Inserted Ruthenium Oxide," *J. Electrochem. Soc.*, **145** (1), 49 (1998).

6. A. Yoshida and K. Imoto, *Electric Double Layer Capacitor and Method for Producing the Same*, U.S. patent No. 5,150,283, issued to Matsushita Electric Industrial Co., Japan (September 22, 1992).

7. J. P. Zheng, J. Huang, and T. R. Jow, "The Limitations of Energy Density for Electrochemical Capacitors," *J. Electrochem. Soc.*, **144**(6), 2026 (1997).

8. J. P. Zheng and T. R. Jow, "The Effect of Salt Concentration in Electrolytes on the Maximum Energy Storage for Double Layer Capacitors," *J. Electrochem. Soc.*, **144**(7), 2417 (1997).

9. M. Morita, M Goto, and Y. Matsuda, "Ethylene Carbonate-Based Organic Electrolytes for Electric Double Layer Capacitors," *J. Appl. Electrochemistry*, **22**, 901 (1992).

10. C. J. Farahmandi and J. M. Dispennette, *High Performance Double Layer Capacitors Including Aluminum Carbon Composite Electrodes*, U.S. patent No. 5,621,607, issued to Maxwell Laboratories, Inc., USA (April 15, 1997).

11. M. Ue, M. Takeda, M. Takehara, and S. Mori, "Properties of New Quaternary Ammonium Salts for Electrochemical Capacitors," *Electrochemical Capacitor II*, **PV96-25**, The Electrochemical Society Proceedings Series, Pennington, NJ (1997).

12. M. Ue, M. Takeda, M. Takehara, and S. Mori, "Electrochemical Properties of Quaternary Ammonium Salts for Electrochemical Capacitors," *J. Electrochem. Soc.*, **144**, 2684 (1997).

13. M. Ue, K. Ida, and S. Mori, "Electrochemical Properties of Organic Liquid Electrolytes Based on Quaternary Onium Salts for Electrical Double Layer Capacitors," *J. Electrochem. Soc.*, **141**, 2989 (1994).

14. A. B. McEwen, H. L. Ngo, J. L. Goldman, T. Blakley, and W. F. Averill, "Nonaqueous Electrolytes and Novel Packaging Concepts for Electrochemical Capacitors," *The 7th International Seminar on Double Layer Capacitors and Similar Energy Storage Devices*, Deerfield Beach, FL (December 8–10, 1997).

15. A. B. McEwen, S. F. McDevitt, and V. R. Koch, *J. Electrochem. Soc.,* **144**, L84 (1997).

16. A. B. McEwen, R. Chadha, T. Blakley, and V. R. Koch, *Electrochemical Capacitor II*, **PV96-25**, The Electrochemical Society Proceedings Series, Pennington, NJ (1997), p 313.

17. J. Fuller, R. T. Carlin, and R. A. Osteryong, "The Room Temperature Ionic Liquid 1-Ethyl-3-Methylimindazolium Teterafluoroborate: Electrochemical Couples and Physical Properties," *J. Electrochem. Soc.,* **144**, 3881 (1997).

18. V. R. Koch, L. A. Dominey, C. Nanjundiah, and M. J. Ondrechen, *J. Electrochem. Soc.,* **143**, 788 (1996).

19. J. March, *Advanced Organic Chemistry*, 3rd ed., John Wiley & Sons, New York (1985).

20. H. House, *Modern Synthetic Chemistry*, 2nd ed., W. A. Benjamin, Menlo Park, CA (1992).

21. Houben-Weyl, *Methoden der organischen Chemie*, Bd. IX, Thieme Verlag, Stuttgart (1995).

22. A. Hiers, *Organic Synthesis*, John Wiley & Sons, New York (1932).

23. S. Mori, K. Ida, M. Ue, *Process for Producing Quaternary Salts*, U.S. patent No. 4,892,944 (1990).

24. D. Linden, *Handbook of Batteries*, 2nd ed., McGraw-Hill, New York (1994).

25. S. P. Ding, K. Xu, and T. R. Jow, "Comparison of Properties of a Symmetric and Asymmetric Tetraalkylammonium Salt and Their Nonaqueous Electrolytes," *Proceedings of the Symposium on Batteries for the 21st Century,* the 194th Meeeting of The Electrochemical Society, Boston, MA (November 1–6, 1998).

26. C. Kittel, *Introduction to Solid State Physics*, 6th ed., John Wiley & Sons, Inc., New York (1986) p 67.

27. K. Xu, S. P. Ding, and T. R. Jow, "Quaternary Ammonium and Phosphonium Salts and Evaluation of Electrochemical Stability in Double Layer Capacitors" submitted to *J. Electrochem. Soc.*

28. S. P. Ding, K. Xu, and T. R. Jow, "Conductivity of Asymmetric Quaternary Ammonium Salts in Binary Carbonates," to be submitted to *J. Electrochem. Soc*.

29. A. B. McEwen, H. L. Ngo, J. L. Goldman, T. Blakley, and W. F. Averill, "Nonaqueous Electrolytes and Novel Packaging Concepts for Electrochemical Capacitors," *Proceedings of the 7th International Seminar on Double Layer Capacitors and Similar Energy Storage Devices*, Deerfield Beach, FL (December 8–10, 1997).

30. K. Xu, S. P. Ding, and T. R. Jow, "Toward Reliable Values of Electrochemical Stability Limits for Electrolytes," submitted to *J. Electrochem. Soc.*

31. S. Hirahara, K. Okuyama, M. Suzuki, K. Matsuura, and Y. Takeda, "High Energy Density Double-Layer Capacitor by Li-Doping Techniques," *Abstract No. 82*, The 194th Meeting of the Electrochemical Society, Boston, MA (November 1–6, 1998).